Desalination and Water Treatment
www.deswater.com
doi: 10.1080/19443994.2014.911705

54 (2015) 3300–3310
June

Taylor & Francis
Taylor & Francis Group

Application of response surface methodology for optimization of operational variables in photodegradation of phenazopyridine drug using TiO_2/CeO_2 hybrid nanoparticles

Hamed Eskandarloo[a], Alireza Badiei[a,*], Mohammad A. Behnajady[b]

[a]*School of Chemistry, College of Science, University of Tehran, Tehran, Iran, Tel. +98 2161112614; Fax: +98 2161113301; Email: abadiei@ut.ac.ir*
[b]*Department of Chemistry, College of Science, Tabriz Branch, Islamic Azad University, Tabriz, Iran*

Received 12 September 2013; Accepted 25 March 2014

ABSTRACT

In the present work, a powder mixture of the TiO_2 and CeO_2 solid oxides was used for preparation of TiO_2/CeO_2 hybrid nanoparticles. Crystallite size and structure of prepared TiO_2/CeO_2 hybrid nanoparticles were determined by X-ray diffraction and transmission electron microscopy techniques. The effect of operational variables such as catalyst dosage, initial drug concentration, irradiation time, and distance of the solution from UV lamp was predicted and optimized in the photocatalytic removal of phenazopyridine (PhP) using response surface methodology. The results showed that the predicted values of removal efficiency were found to be in good agreement with the experimental results with a correlation coefficient (R^2) of 0.9542. The optimum operational conditions were found to be: catalyst dosage of 0.41 g L^{-1}, initial drug concentration of 6.61 mg L^{-1}, irradiation time of 30 min, and distance of the solution from UV lamp of 2 cm. Under the optimized conditions, the maximum removal rate (97.74%) of PhP was achieved.

Keywords: Titanium dioxide; Photocatalytic removal; Phenazopyridine drug; Optimization; Operational variables; Response surface methodology

1. Introduction

Environmental pollution and destruction on a global scale, as well as the shortage of sufficient clean and natural energy sources, have attracted much attention to the vital need for developing ecologically clean and safe chemical technology, materials, and processes [1]. The heterogeneous photocatalysis process represents one of advanced oxidation processes (AOPs) that provide an interesting route to the destruction of many organic substances to CO_2, H_2O, and corresponding mineral acids [2]. Heterogeneous photocatalysis involves combination of UV light and a catalyst usually in suspension mode in aqueous solution. When materials such as TiO_2 and ZnO absorb a photon with energy greater than or equal to the band gap energy leads to produce electron–hole pairs within the conduction and valence bands [3,4]. Generated electron–hole pairs can either recombine and release heat energy or interact separately with other molecules [3]. Reactions between adsorbed water, hydroxyl anions, and oxygen molecules or other substances with electron and hole pairs produced at the catalyst surface under UV irradiation produce

*Corresponding author.

hydroxyl radicals. The hydroxyl radical is a powerful oxidizing agent and attacks organic compounds [5]. In order to reduce electron–hole recombination, various methods have been conducted, including coupling materials and doping of transition metal and rare earth metal ions [6,7]. Coupling TiO_2 with electron-accepting materials can greatly enhance the photocatalytic activity of hybrid systems [8,9]. There have been a lot of studies related to TiO_2 coupled with other metal oxides [10]. Among them, coupling TiO_2 with CeO_2 attracts much attention, due improves textural and structural properties of TiO_2 [11,12]. TiO_2 and CeO_2 coupling can produce a special electrons and holes transfer from TiO_2 to CeO_2, which is able to facilitate the separation of the electron–hole pairs and thus improve photocatalytic activity of the hybrid nanoparticles [13].

In the present work, a powder mixture of the TiO_2 and CeO_2 solid oxides was used for preparation of TiO_2/CeO_2 hybrid nanoparticles and the effect of various operational variables was optimized in the photocatalytic removal of phenazopyridine (PhP) as a model drug contaminant using response surface methodology (RSM) technique. RSM is a mathematical and statistical technique that is widely employed in process optimizing and modeling. RSM technique is capable of analyzing the interactions of possible influencing factors, and determining the optimum region of the factors level with just using minimum number of designed experiments [14,15]. Box–Behnken and central composite design (CCD) are the most commonly selected methods in RSM technique [16]. PhP is a widely used analgesic drug which relieves urinary tract pain, burning, irritation, and discomfort [17]. Effect of operational variables on the removal efficiency of PhP was established by the response surface and contour plots.

2. Materials and methods

2.1. Materials

The following analytical grade chemicals were used without any further purification: TiO_2 (pure anatase phase, BET surface area 10 m^2/g, CAS number 13463-67-7) and cerium dioxide (CAS number 1306-38-3) powders were purchased from Merck Co. (Germany). PhP ($C_{11}H_{11}N_5$.HCl, molar mass of 249.7 g/mol, CAS number 94-78-0) was kindly donated by Tehran pharmaceutical company (Iran). Molecular structure of PhP is given in Fig. 1.

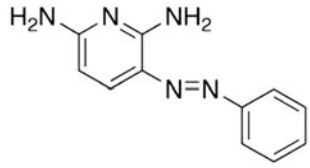

Fig. 1. Molecular structure of PhP.

2.2. Preparation of TiO_2/CeO_2 hybrid nanoparticles

A powder mixture of the TiO_2 and CeO_2 solid oxides was used for preparation of TiO_2/CeO_2 hybrid nanoparticles, according to the following steps. First, 1 g of TiO_2 and CeO_2 powders mixture with 0.8:0.2 weight ratio of Ti:Ce was ground thoroughly in an agate mortar and added to 100 mL boiling deionized water. Then the mixed oxides were dispersed in 100 mL boiling deionized water and sonicated for 15 min using a probe sonicator (Bandelin HD 3200, 200 W). The suspension solution was stirred for 24 h and then dried in an air oven at 80 °C for about 12 h. Finally, the dried solids were calcined at 500 °C for 60 min.

2.3. Characterization of photocatalysts

Structure and crystallite size of TiO_2/CeO_2 hybrid nanoparticles were analyzed by X-ray diffraction (XRD) measurements which was carried out at room temperature by using Philips X'pert MPD diffractometer with Cu Kα radiation ($\lambda = 0.15478$ nm). The (101) reflection ($2\theta = 25.28^\circ$) of anatase TiO_2 and the (111) reflection ($2\theta = 28.8^\circ$) of cubic CeO_2 were used for analysis. The average crystallite size (D in nm) of TiO_2 anatase phase and CeO_2 cubic structure in hybrid nanoparticles were calculated from XRD diffraction reflections using the Scherrer's method, according to Eq. (1) [18]:

$$D = \frac{k\lambda}{\beta \cos\theta} \quad (1)$$

where k is a constant equal to 0.89, λ the X-ray wavelength equal to 0.154056 nm, β the full width at half maximum intensity, and θ the half diffraction angle.

Size of the synthesized TiO_2 nanoparticles was obtained by transmission electron microscopy (TEM) instrument (EM 208 Philips, 100 kV).

2.4. Photocatalysis experiments

Removal of PhP from aqueous solution was carried out at room temperature in a batch quartz reactor. Artificial irradiation was provided by a 15 W (UV-C, light intensity of 56.5 W m^{-2} in front of the reactor) mercury lamp (Philips, Holland) emitting around 254 nm, positioned in top of the batch quartz reactor. The light intensity was measured using a Lux-UV-IR meter (Leybold, Germany). In each run, desired amount of photocatalyst (0.24, 0.32, 0.4, 0.48, and 0.56 g L^{-1}) was dispersed in 100 mL water for 15 min using a probe sonicator, then desired concentration of PhP (4, 8, 12, 16, and 20 mg L^{-1}) and photocatalyst was transferred into the batch quartz reactor, and was stirred for 30 min to reach the adsorption equilibration in the dark before irradiation. The photocatalytic reaction was initiated with turning on the light source. The optical absorption spectrum of PhP (12 mg L^{-1}) was recorded in the range of 200–600 nm by UV–vis spectrophotometer (Rayleigh UV-1600), and it was found that λ_{max} of PhP is nearly 430 nm. At given irradiation time intervals (10, 15, 20, 25, and 30 min), the samples (5 mL) were taken out, centrifuged (Sigma 2-16P), and then PhP concentration analyzed at 430 nm. Absorption spectrum of aqueous colloidal TiO_2 in the range of UV (334 nm) has been used to ensure that any residual of nanoparticles did not exist in the centrifuged solutions [19]. The results showed that the sample taken out from the centrifuge did not show any absorption.

2.5. Electrical energy determination

In photocatalysis process, electric energy consumption can be a major fraction of the operating costs, therefore simple figures of merit based on electric energy consumption can be very useful and informative. Bolton et al. [20] defined the figures of merit "electric energy per order" (E_{EO}) for using in the first order kinetic regime of AOPs. This concept was accepted by the IUPAC as a technical report. Definition of E_{EO} is the number of kilowatt hours of electrical energy needed to reduce the concentration of a pollutant by one order of magnitude (90%) in a unit volume of contaminated water. The E_{EO} (k/Wh m^{-3} $order^{-1}$) required to the photocatalytic removal of PhP calculated from the following equations [20]:

$$E_{EO} = \frac{P_{el} \times t \times 1,000}{V \times 60 \times \log\left(\frac{[C]_0}{[C]}\right)} \quad (2)$$

$$\ln \frac{[C]}{[C]_0} = -k_{ap} \times t \quad (3)$$

where P_{el} is the input power (kW) to AOP system, k_{ap} is the pseudo-first-order reaction rate constant (min^{-1}), t is the irradiation time (min), V is the volume of water (L) in the reactor, and $[C]_0$ and $[C]$ are the initial and final concentrations of PhP, respectively. The k_{ap} for each process was estimated from the slope of plot of ln ($[C_0]/[C]$) against process time (t) vs. reaction time. For a pseudo-first-order reaction in a batch reactor, E_{EO} can be written as follows [20]:

$$E_{EO} = \frac{38.4 \times P_{el}}{V \times k_{ap}} \quad (4)$$

2.6. Experimental design

In the present study, CCD was used to propose and estimate a mathematical model of the photocatalytic process behavior. Computational analysis of the experimental data was supported by the Design-Expert (version 7) software. In order to evaluate the effect of independent operational variables, four key factors were chosen: photocatalyst dosage (g L^{-1}), initial drug concentration (mg L^{-1}), irradiation time (min), and distance of the solution from UV lamp (cm) and the photocatalytic removal efficiency of PhP was selected as the response. A total of 31 experiment runs were performed in this work with seven replications at the center point. For statistical calculations, four chosen operational variables were converted to dimensionless ones (x_1, x_2, x_3, x_4), with the coded values at levels: –2, –1, 0, +1, and +2. The experimental ranges and the levels of the operational variables are presented in Table 1.

Table 1
Experimental ranges and levels of the operational variables

Operational variables	Symbol x_i	Ranges and levels				
		–2	–1	0	+1	+2
Catalyst dosage (g L^{-1})	x_1	0.24	0.32	0.4	0.48	0.56
Initial drug concentration (mg L^{-1})	x_2	4	8	12	16	20
Irradiation time (min)	x_3	10	15	20	25	30
Distance between UV lamp and the solution (cm)	x_4	2	4	6	8	10

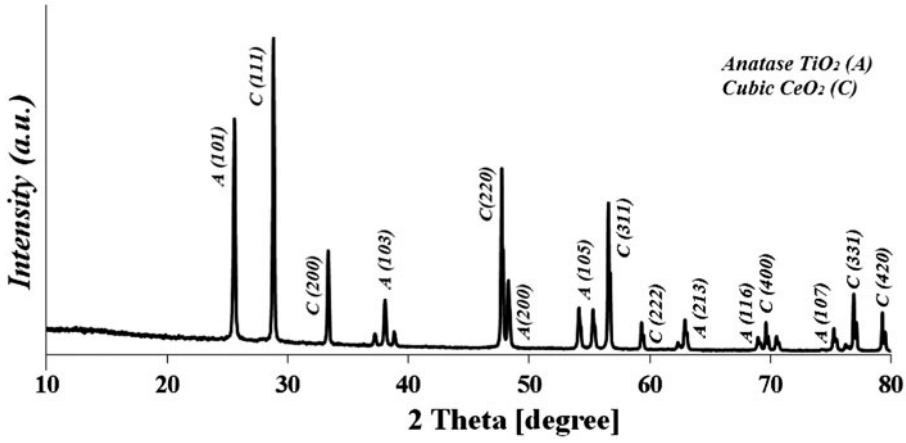

Fig. 2. XRD pattern for TiO_2/CeO_2 hybrid nanoparticles.

3. Results and discussion

3.1. Characterization of TiO_2/CeO_2 hybrid nanoparticles

Fig. 2 depicts the XRD patterns of TiO_2/CeO_2 nanoparticles. The reflections in XRD at 2θ of 25.4°, 36.9°, 38.2°, 37.9°, 48.1°, 54°, 55.2°, and 62.8° are attributed to anatase phase of TiO_2 and reflections at 2θ of 28.6, 33.21°, 47.6°, 56.5°, 59.2°, 69.5°, 76.8°, and 79.2° are attributed to CeO_2. No rutile phase reflection of TiO_2 was observed for the prepared TiO_2/CeO_2 nanoparticles. The average crystallite size of the TiO_2/CeO_2 hybrid nanoparticles calculated using the Scherrer's equation was in the range of 21–34 nm. The TEM image of the TiO_2/CeO_2 hybrid nanoparticles is shown in Fig. 3. The average particle size of the TiO_2/CeO_2 nanoparticles was found to be <40 nm, which is in agreement with the crystallite size calculated from the XRD pattern.

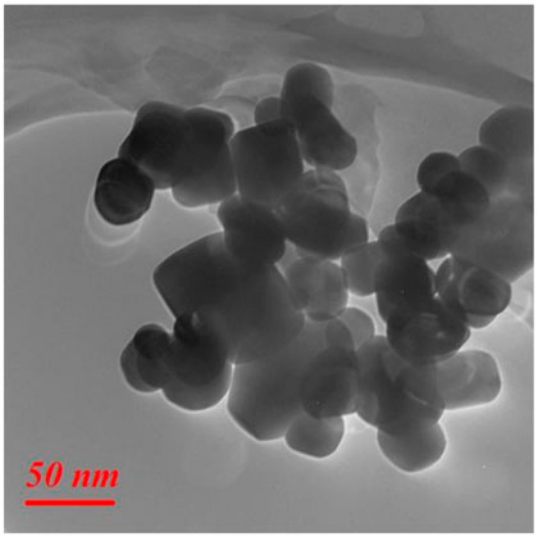

Fig. 3. TEM image of TiO_2/CeO_2 hybrid nanoparticles.

3.2. Photocatalytic activity and optimization of operational variables

3.2.1. Model results

The mathematical relationship between the response and these variables can be approximated by the following second-order polynomial Eq. (5):

$$Y = b_0 + b_1x_1 + b_2x_2 + b_3x_3 + b_4x_4 + b_{12}x_1x_2 + b_{13}x_1x_3 + b_{14}x_1x_4 + b_{23}x_2x_3 + b_{24}x_2x_4 + b_{34}x_3x_4 + b_{11}x_1^2 + b_{22}x_2^2 + b_{33}x_3^2 + b_{44}x_4^2 \quad (5)$$

where Y is a predicted response of photocatalytic removal efficiency, b_0 is the constant, b_1, b_2, b_3, and b_4 are the regression coefficients for linear effects, b_{12}, b_{13}, b_{14}, b_{23}, b_{24}, and b_{34} are the regression coefficients for interaction effects, $b_1{}^2$, $b_2{}^2$, $b_3{}^2$, and $b_4{}^2$ are the regression coefficients for squared effects, and x_i is coded experimental levels of the operational variables.

The details of the designed experiments along with experimental results and predicted values for photocatalytic removal efficiencies of PhP drug are presented in Table 2. Based on these results, an empirical relationship between the response (Y) and independent operational variables (x_1, x_2, x_3, x_4, see Table 1) was attained as shown in Eq. (6):

Table 2
The 4-factor CCD matrix with the experimental and predicted responses

Run	$[TiO_2/CeO_2]_0$ ($g\,L^{-1}$)	$[Drug]_0$ ($mg\,L^{-1}$)	Irradiation time (min)	Distance from UV lamp (cm)	RE (%)	
					Experimental	Predicted
1	0.24	12	20	6	59.61	59.73
2	0.32	8	25	8	60.57	60.03
3	0.48	16	15	4	50.94	51.83
4	0.40	12	20	6	66.24	66.42
5	0.40	12	20	2	86.28	79.54
6	0.40	20	20	6	45.01	46.83
7	0.40	12	30	6	72.65	72.48
8	0.32	8	15	8	54.62	53.11
9	0.40	12	20	6	66.35	66.42
10	0.32	16	15	4	60.64	62.97
11	0.48	8	25	4	81.01	83.67
12	0.32	16	25	4	71.86	71.02
13	0.40	12	20	6	66.66	66.42
14	0.48	8	15	8	61.39	62.58
15	0.40	12	10	6	57.89	56.69
16	0.40	12	20	6	66.16	66.42
17	0.32	16	15	8	50.49	48.17
18	0.40	12	20	6	66.81	66.42
19	0.32	8	25	4	78.77	81.31
20	0.40	12	20	10	46.02	51.38
21	0.48	8	15	4	71.17	73.31
22	0.40	12	20	6	66.09	66.42
23	0.32	16	25	8	54.72	53.6
24	0.48	16	25	8	53.44	51.2
25	0.40	4	20	6	77.94	74.74
26	0.40	12	20	6	66.64	66.42
27	0.48	8	25	8	71.62	70.31
28	0.32	8	15	4	69.18	71.77
29	0.48	16	15	8	46.49	44.96
30	0.56	12	20	6	60.37	58.88
31	0.48	16	25	4	58.18	60.7

$$Y = 66.42 - 0.21x_1 - 6.98x_2 + 3.95x_3 - 7.04x_4 - 3.17x_1x_2 + 0.2x_1x_3 + 1.98x_1x_4 - 0.37x_2x_3 + 0.97x_2x_4 - 0.66x_3x_4 - 1.78x_1^2 - 1.41x_2^2 - 0.46x_3^2 - 0.24x_4^2 \quad (6)$$

Eq. (6) is used to predict the photocatalytic removal efficiencies of PhP by the TiO_2/CeO_2 hybrid nanoparticles with varied operational variables within the selected experimental ranges. Using second-order polynomial equation (Eq. (6)), the predicted values of photocatalytic removal of PhP are plotted vs. corresponding experimental results in Fig. 4. Results confirm that the predicted photocatalytic removal efficiencies for PhP from the model are in good agreement with the experimental results.

Analysis of variance (ANOVA) of the quadratic response surface model is a statistical procedure to test the significance and adequacy of the model [21]. Table 3 shows the ANOVA results for quadratic response surface model. According to the ANOVA results, the regression model presents a high correlation coefficients ($R^2 = 0.9542$) for the photocatalytic removal of PhP. The value of R^2 implies a satisfactory representation of photocatalytic removal process by the model. Adjusted R^2 is also used to measure the goodness of fit between model and experimental data. The effect of independent operational variables with adjusted R^2 value (0.9138) was very close to the corresponding R^2 value. The F value is the ratio between the mean square of the model and the residual error, and indicates the significance of each controlled factor on the tested model [22]. The F value for the models

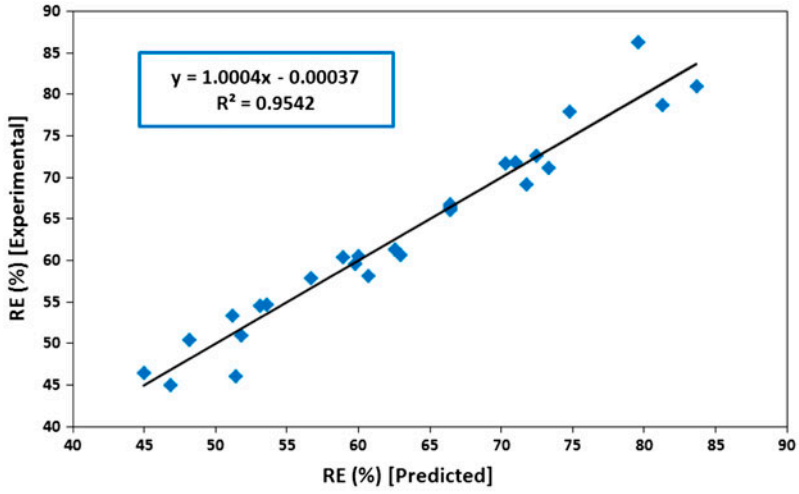

Fig. 4. Comparison between predicted and experimental removal efficiencies of PhP by TiO_2/CeO_2 hybrid nanoparticles.

Table 3
ANOVA results of the response surface quadratic model for the photocatalytic removal of PhP

Source of variations	Sum of squares	Degree of freedom	Mean square	*F*-value	*p*-value
Regression	3115.16	14	222.51	23.73	<0.0001
Residual	150.05	16	9.38		
Total	3265.21	30			

Note: $R^2 = 0.9540$, adjusted $R^2 = 0.9138$.

is 23.73 and the corresponding *p*-value is <0.0001. These results indicated that the model was statistically significant and there is only a 0.01% chance that the "model *F*-value" could occur due to noise.

3.2.2. Effect of operational variables as response surface and contour plots

The response surface and contour plots for operational variables, while two variable kept at constant and the others varying within the experimental ranges, are obtained. In order to find out the effect of catalyst dosage on photocatalytic removal efficiency of PhP, the experiments were carried out with catalyst dosage varying in the range of 0.24–0.56 g L^{-1} at initial drug concentration of 12 mg L^{-1} and 6 cm distance of the solution from UV lamp. Fig. 5 shows the effect of the catalyst dosage and irradiation time on the removal efficiency of PhP. It could be seen from this figure that the increase in the TiO_2/CeO_2 dosage from 0.24 to 0.4 g L^{-1} improves the removal efficiency of PhP from 59.6 to 66.35%. This can be the result of increasing of available adsorption and catalytic sites on the TiO_2/CeO_2 surface, which are responsible for photocatalytic activity [23–25]. Therefore, the formation of $^{\bullet}OH$ and adsorption of PhP molecules on TiO_2/CeO_2 surface increase and consequently photocatalytic removal efficiency will be enhanced. As it is clear from the Fig. 5, improvement on removal efficiency is not obvious above 0.4 g L^{-1}, because higher catalyst loading cause higher agglomeration (particle/particle interaction) and turbidity of suspension, consequently reduces the available surface area for absorbing the PhP molecules and scattering effect increases which causes a decrease in UV light penetration to the solution [26–29]. The same observation was reported for the photocatalytic degradation of methyl orange using ZnO–SnO_2 nanoparticles by Behnajady and Tohidi [30]. They were reported that 800 mg L^{-1} is as an optimum dosage of ZnO–SnO_2 nanoparticles for the photocatalytic degradation of methyl orange. The contour plots show that the optimum region for PhP removal efficiency is the catalyst dosage range of 0.32–0.48 g L^{-1}. On the other hand, removal efficiency of drug increased with increasing photocatalytic irradiation time. For all catalyst dosage, highest removal efficiency was obtained after irradiation time of 30 min. It is obvious that catalyst dosage effect on PhP removal is less significant relative to the irradiation time.

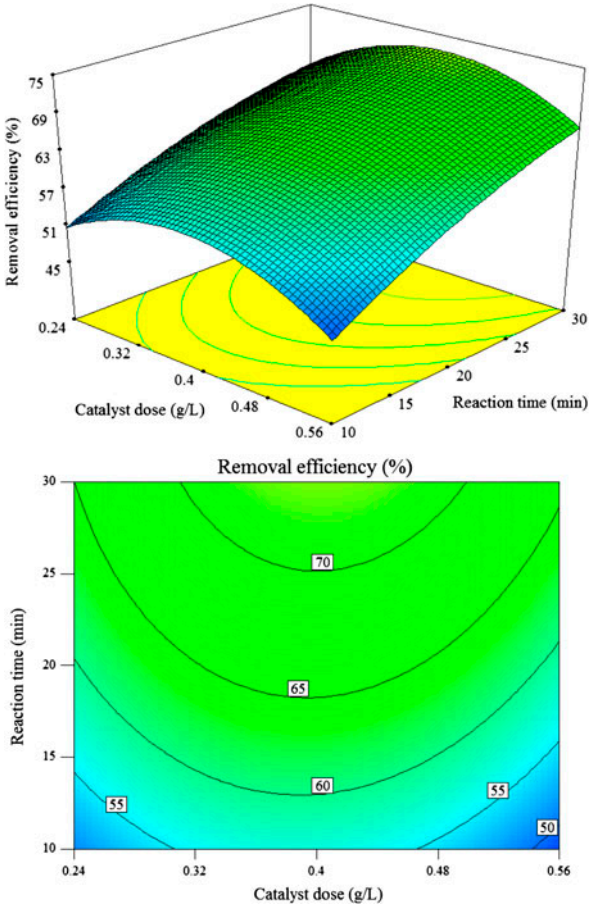

Fig. 5. The response surface plots and contour plots of the removal efficiency of PhP by TiO_2/CeO_2 hybrid nanoparticles as a function of catalyst dosage and irradiation time.

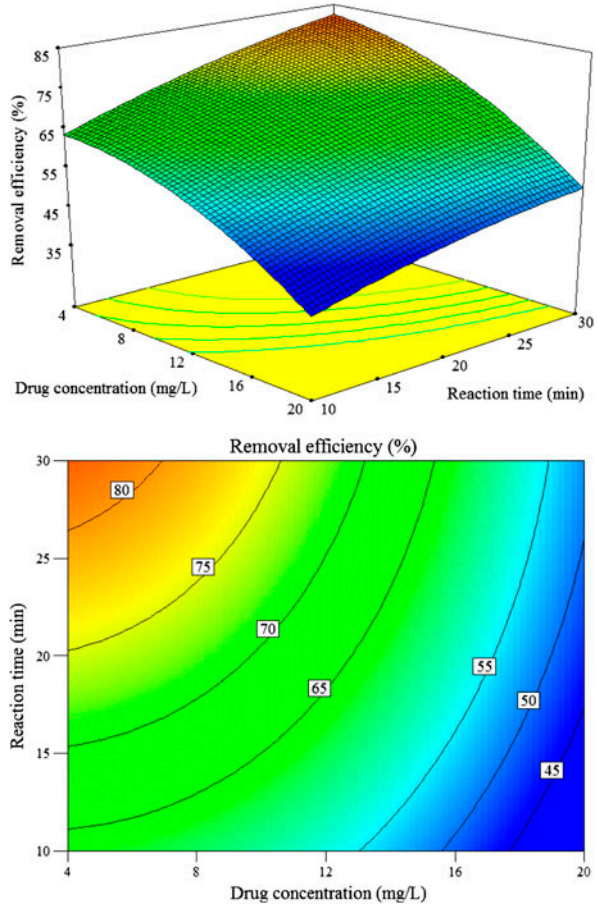

Fig. 6. The response surface and contour plots of the removal efficiency of PhP by TiO_2/CeO_2 hybrid nanoparticles as a function of initial PhP concentration and irradiation time.

It is important from an application point of view to study the dependence of photocatalytic removal efficiency on the initial concentration of drug. Fig. 6 shows the effect of the initial PhP concentration and irradiation time on the removal efficiency of PhP for catalyst dosage of 0.4 g L^{-1} and 6 cm distance of the solution from UV lamp. It is observed in Fig. 6 that the decrease in the initial amount of drug from 20 to 4 mg L^{-1} improves the removal efficiency from 45.01 to 77.94%. This can be the result of following reasons: one explanation is that with increasing of drug concentration more and more organic substances (PhP and intermediates molecules) are adsorbed on the surface of TiO_2/CeO_2 catalysts, therefore the generation of active species such as hydroxyl radicals will be reduced [31–33]. For higher PhP concentration, more reactive radical species such as $^{\bullet}OH$ and $O_2^{-\cdot}$ are needed, but at a fixed operational conditions (TiO_2/CeO_2 dosage, irradiation time, and light intensity), the formation of $^{\bullet}OH$ and $O_2^{-\cdot}$ species will be kept at a fixed level, thus, the removal efficiency of PhP will be reduced [34]. Another explanation is that the molar extinction coefficient of the PhP in UV–vis regions is very high, so that its concentration increases, causing an inner filter effect. Thus, with increasing of drug concentration, the solution becomes impermeable to UV radiation, so the photons get intercepted before they can reach the catalyst surface [35–38]. The same observations were reported for the photocatalytic degradation of leather dye on TiO_2 by Macedo et al. [39] and for the photocatalytic degradation of Basic Red 46 dye on TiO_2 by Zarei et al. [40]. The contour plots show that the optimum region for PhP removal efficiency is the initial drug concentration range of about 4–6 mg L^{-1}. The highest drug removal efficiency (≥80%) is achieved using minimum value for initial drug concentration and maximum value for irradiation time, when catalyst dosage and distance of the solution from UV lamp variables kept at constant 0.4 g L^{-1} and 6 cm.

Fig. 7 shows the effect of the distance between UV lamp and the solution and irradiation time on the removal efficiency of drug for 0.4 g L^{-1} catalyst dosage and 12 mg L^{-1} initial drug concentration. As can be seen from the response surface and contour plots, removal efficiency of PhP decreased from 86.28 to 46.02% with increasing the distance between UV lamp and the solution from 2 to 10 cm. Because the UV light irradiation generates the photons needed for the electron transfer from the valence band to the conduction band of a photocatalyst. Herrmann reported that at low light intensities, the photocatalytic removal rate is dependent of light intensity and would increase linearly with increasing light intensity [41]. When the light intensity is low, electron–hole separation competes with recombination and decreases the formation of hydroxyl radicals [42–44]. Whereas, at intermediate light intensities, the photocatalytic removal rate would depend on the square root of the light intensity and at high light intensities the photocatalytic removal rate is independent of light intensity [34,41,45]. The removal rate of PhP increases when more radiations fall on the catalyst surface and hence more hydroxyl radicals are produced [42–44]. These observations are in accordance with those obtained by other literature studies. For example, decreased removal rate by decreasing UV light intensity was reported for photocatalytic degradation of diazo Direct Yellow 12 using TiO_2 catalyst, by Toor et al. [46]. Behnajady et al. was reported that the photocatalytic degradation of Acid Red 88 using immobilized ZnO increased by increasing light intensity [47]. The highest drug removal efficiency (≥85%) by TiO_2/CeO_2 hybrid nanoparticles is achieved when distance between UV lamp and the solution and irradiation time is maintained at their minimum and maximum values, respectively.

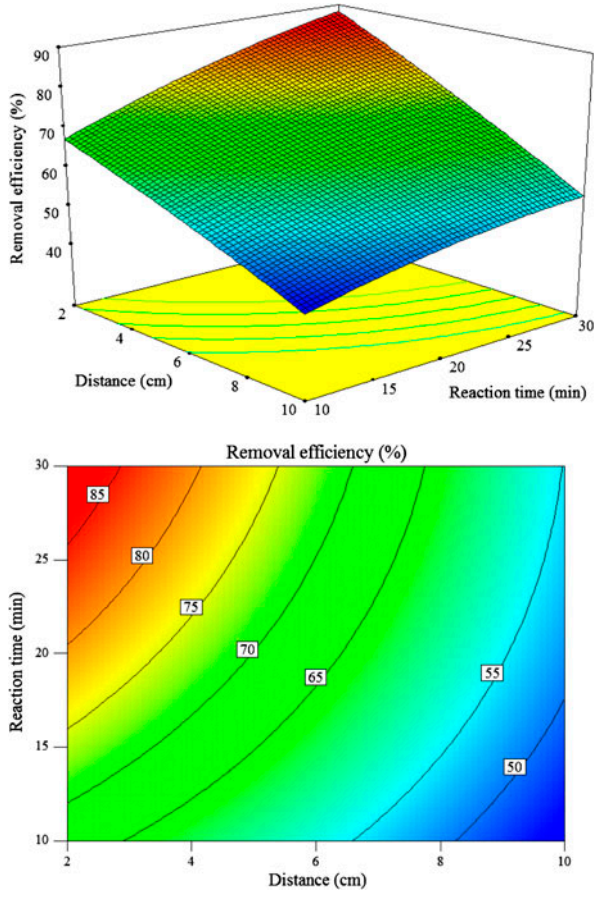

Fig. 7. The response surface plots and contour plots of the removal efficiency of PhP by TiO_2/CeO_2 hybrid nanoparticles as a function of distance of solution from UV lamp and irradiation time.

3.2.3. Determination of optimal conditions for operational variables

The photocatalytic removal efficiency of PhP was defined as "maximize" to achieve optimum values of operational variables in the selected range that the catalyst dosage, initial drug concentration, irradiation time, and distance from UV lamp are in the range of 0.24–0.56 g L^{-1}, 4–20 mg L^{-1}, 10–30 min, and 2–10 cm, respectively. The optimal conditions of the operational variables for the maximum photocatalytic removal efficiency with predicted and observed RE% are shown in Table 4. The optimum values of operational variables for photocatalytic removal efficiency of PhP are 0.41 g L^{-1}, 6.61 mg L^{-1}, 2 cm, and 30 min for catalyst dosage, initial drug concentration, irradiation time, and distance from UV lamp, respectively. As a consequent, experimental design strategy can be a successful investigation to determine the optimum values of operational variables and can be an adequate modeling to predict photocatalytic removal efficiency.

The pseudo-first-order reaction rate constant for the photocatalytic removal of PhP was 0.151 min^{-1}, and accordingly electrical energy required calculated using the Eq. (4) was 38.15 k/Wh m^{-3} $order^{-1}$. It is useful to relate the values of electrical energy found in this work to the operation costs. By considering 0.036 US $/k/Wh as the cost of electricity in Iran, the contribution to operation costs of PhP removal for electrical energy will be 1.37 US $/$m^3$. Daneshvar et al. reported that the E_{EO} values required for removal of Acid Orange 7 under UV irradiation in the presence of ZnO and ZnO/H_2O_2 were 384 and 172 k/Wh m^{-3} $order^{-1}$, respectively [48]. Esen et al. reported that the E_{EO} values required for decolorization of malachite green and titanium yellow under UV light in the

Table 4
Optimum values of the operational variables for maximum photocatalytic removal efficiency of PhP

Catalyst dosage ($g\,L^{-1}$)	Initial drug concentration ($mg\,L^{-1}$)	Irradiation time (min)	Distance from UV lamp (cm)	Predicted RE (%)	Observed RE (%)
0.41	6.61	30	2	98.68	97.74

presence of SnO_2 nanoparticles (catalyst amount, 50 mg) were 72 and 8,620 $k/Wh\,m^{-3}\,order^{-1}$, respectively [49]. Khataee et al. studied the removal of Acid Blue 9 under UV light illumination (30 W) in the presence of TiO_2 nanoparticles with different crystalline forms: anatase, rutile, and mixed-phase (70% anatase), and they reported that the E_{EO} values required were 3,439, 1,449, and 616 $k/Wh\,m^{-3}\,order^{-1}$, respectively [50]. According to these result, less energy was consumed during the removal of PhP in the presence of TiO_2/CeO_2 hybrid nanoparticles under the optimized conditions in comparison to other studies. This is a significant consideration in view of the evaluation of the treatment costs for the industrial applications as electric energy can correspond to a major fraction of the operating costs.

4. Conclusions

We have successfully prepared TiO_2/CeO_2 hybrid nanoparticles with crystallite size between 30 and 40 nm and the photocatalytic activity of TiO_2/CeO_2 hybrid nanoparticles was studied in the removal of PhP under UV light. RSM was successfully employed in this study to optimize the individual and interaction effects of the operational parameters. The results showed that the predicted values of removal efficiency were found to be in good consistency with experimental results with a correlation coefficient (R^2) of 0.9542. Optimization results showed that maximum removal efficiency (97.74%) was achieved at the operational conditions: catalyst dosage of 0.41 $g\,L^{-1}$, initial drug concentration of 6.61 $mg\,L^{-1}$, irradiation time of 30 min, and 2-cm distance from UV lamp. The results clearly demonstrated that RSM with a CCD was one of the reliable methods to modeling and optimizing of the operational variables. The electrical energy consumption was calculated and results showed that the less energy was consumed during the removal of PhP in the presence of TiO_2/CeO_2 hybrid nanoparticles under the optimized conditions.

Acknowledgment

The authors thank University of Tehran for the supporting this work.

References

[1] M. Anpo, S. Dohshi, M. Kitano, Y. Hu, M. Takeuchi, M. Matsuoka, The preparation and characterization of highly efficient titanium oxide-based photofunctional materials, Annu. Rev. Mater. Res. 35 (2005) 1–27.
[2] M.A. Behnajady, H. Eskandarloo, N. Modirshahla, M. Shokri, Influence of the chemical structure of organic pollutants on photocatalytic activity of TiO_2 nanoparticles: Kinetic analysis and evaluation of electrical energy per order (E_{EO}), Dig. J. Nanomater. Bios. 6 (2011) 1887–1895.
[3] A. Fujishima, K. Honda, Electrochemical photolysis of water at a semiconductor electrode, Nature 238 (1972) 37–38.
[4] M.A. Behnajady, H. Eskandarloo, Silver and copper co-impregnated onto TiO_2-P25 nanoparticles and its photocatalytic activity, Chem. Eng. J. 228 (2013) 1207–1213.
[5] N. Daneshvar, M. Rabbani, N. Modirshahla, M.A. Behnajady, Kinetic modeling of photocatalytic degradation of Acid Red 27 in UV/TiO_2 process, J. Photochem. Photobiol., A 168 (2004) 39–45.
[6] K.M. Parida, N. Sahu, Visible light induced photocatalytic activity of rare earth titania nanocomposites, J. Mol. Catal. A: Chem. 287 (2008) 151–158.
[7] M.A. Behnajady, H. Eskandarloo, Characterization and photocatalytic activity of Ag–Cu/TiO_2 nanoparticles prepared by sol–gel method, J. Nanosci. Nanotechnol. 13 (2013) 548–553.
[8] J. Liqiang, F. Honggang, W. Baiqi, W. Dejun, X. Baifu, L. Shudan, S. Jiazhong, Effects of Sn dopant on the photoinduced charge property and photocatalytic activity of TiO_2 nanoparticles, Appl. Catal., B 62 (2006) 282–291.
[9] D. Beydoun, R. Amal, G. Low, S. McEvoy, Role of nanoparticles in photocatalysis, J. Nanopart. Res. 1 (1999) 4394–4358.
[10] S.G. Kumar, L.G. Devi, Review on modified TiO_2 photocatalysis under UV/visible light: Selected results and related mechanisms on interfacial charge carrier transfer dynamics, J. Phys. Chem. A 115 (2011) 13211–13241.
[11] S. Ghasemi, S. Rahman Setayesh, A. Habibi-Yangjeh, M.R. Hormozi-Nezhad, M.R. Gholami, Assembly of CeO_2–TiO_2 nanoparticles prepared in room temperature ionic liquid on graphene nanosheets for photocatalytic degradation of pollutants, J. Hazard. Mater. 199–200 (2012) 170–178.
[12] H. Liu, M. Wang, Y. Wang, Y. Liang, W. Cao, Y. Su, Ionic liquid-templated synthesis of mesoporous CeO_2–TiO_2 nanoparticles and their enhanced photocatalytic activities under UV or visible light, J. Photochem. Photobiol., A 223 (2011) 157–164.
[13] T. Cao, Y. Li, C. Wang, L. Wei, C. Shao, Y. Liu, Three-dimensional hierarchical CeO_2 nanowalls/TiO_2 nanofibers heterostructure and its high photocatalytic performance, J. Sol–Gel Sci. Technol. 55 (2010) 105–110.

[14] C.J. Silva, I.C. Roberto, Optimization of xylitol production by *Candida guilliermondii* FTI 20037 using response surface methodology, Process Biochem. 36 (2001) 1119–1124.
[15] N. Aslan, Application of response surface methodology and central composite rotatable design for modeling and optimization of a multi-gravity separator for chromite concentration, Powder Technol. 185 (2008) 80–86.
[16] C.-H. Dong, X.-Q. Xie, X.-L. Wang, Y. Zhan, Y.-J. Yao, Application of Box–Behnken design in optimisation for polysaccharides extraction from cultured mycelium of *Cordyceps sinensis*, Food Bioprod. Process. 87 (2009) 139–144.
[17] A.S. Gopalachar, V.L. Bowie, P. Bharadwaj, Phenazopyridine-induced sulfhemoglobinemia, Ann. Pharmacother. 39 (2005) 1128–1130.
[18] A.L. Patterson, The scherrer formula for X-ray particle size determination, Phys. Rev. 56 (1939) 978–982.
[19] J.A. Byrne, B.R. Eggins, N.M.D. Brown, B. McKinney, M. Rouse, Immobilisation of TiO_2 powder for the treatment of polluted water, Appl. Catal., B 17 (1998) 25–36.
[20] J.R. Bolton, K.G. Bircger, W. Tumas, C.A. Tolman, Figure-of merit for the technical development and application of advanced oxidation technologies for both electric and solar-derived systems, Pure Appl. Chem. 73 (2001) 627–637.
[21] H.-L. Liu, Y.-R. Chiou, Optimal decolorization efficiency of Reactive Red 239 by UV/TiO_2 photocatalytic process coupled with response surface methodology, Chem. Eng. J. 112 (2005) 173–179.
[22] F. Francis, A. Sabu, K.M. Nampoothiri, S. Ramachandran, S. Ghosh, G. Szakacs, A. Pandey, Use of response surface methodology for optimizing process parameters for the production of α-amylase by *Aspergillus oryzae*, Biochem. Eng. J. 15 (2003) 107–115.
[23] M.A. Behnajady, N. Modirshahla, M. Shokri, H. Elham, A. Zeininezhad, The effect of particle size and crystal structure of titanium dioxide nanoparticles on the photocatalytic properties, J. Environ. Sci. Health., Part A 43 (2008) 460–467.
[24] D. Gümüş, F. Akbal, Photocatalytic degradation of textile dye and wastewater, Water Air Soil Pollut. 216 (2011) 117–124.
[25] M. Shirzad Siboni, M.T. Samadi, J.K. Yang, S.M. Lee, Photocatalytic removal of Cr(VI) and Ni(II) by UV/TiO_2: Kinetic study, Desalin. Water Treat. 40 (2012) 77–83.
[26] L.A. Ghule, A.A. Patil, K.B. Sapnar, S.D. Dhole, K.M. Garadkar, Photocatalytic degradation of methyl orange using ZnO nanorods, Toxicol. Environ. Chem. 93 (2011) 623–634.
[27] M.A. Behnajady, N. Modirshahla, R. Hamzavi, Kinetic study on photocatalytic degradation of C.I. Acid Yellow 23 by ZnO photocatalyst, J. Hazard. Mater. 133 (2006) 226–232.
[28] R. Thiruvenkatachari, S. Vigneswaran, I.S. Moon, A review on UV/TiO_2 photocatalytic oxidation process (Journal Review), Korean J. Chem. Eng. 25 (2008) 64–72.
[29] A.K. Subramani, K. Byrappa, S. Ananda, K.L. Rai, C. Ranganathaiah, M. Yoshimura, Photocatalytic degradation of indigo carmine dye using TiO_2 impregnated activated carbon, Bull. Mater. Sci. 30 (2007) 37–41.
[30] M.A. Behnajady, Y. Tohidi, The effect of operational parameters in the photocatalytic activity of synthesized Mg/ZnO–SnO_2 nanoparticles, Desalin. Water Treat., doi: 10.1080/19443994.2013.852482.
[31] L. Yin, J. Gao, J. Wang, X. Luan, P. Kang, Y. Li, K. Li, X. Zhang, Synthesis of Er^{3+}: $Y_3Al_5O_{12}$ and its effects on the solar light photocatalytic activity of TiO_2–ZrO_2 composite, Res. Chem. Intermed. 38 (2012) 523–536.
[32] M.A. Behnajady, N. Modirshahla, N. Daneshvar, M. Rabbani, Photocatalytic degradation of an azo dye in a tubular continuous-flow photoreactor with immobilized TiO_2 on glass plates, Chem. Eng. J. 127 (2007) 167–176.
[33] X. Bu, G. Zhang, Y. Guo, Thermal modified palygorskite: Preparation, characterization, and application for cationic dye-containing wastewater purification, Desalin. Water Treat. 30 (2011) 39–347.
[34] S. Ahmed, M.G. Rasul, W.N. Martens, R. Brown, M.A. Hashib, Advances in heterogeneous photocatalytic degradation of phenols and dyes in wastewater: A review, Water Air Soil Pollut. 215 (2011) 3–29.
[35] S. Chakrabarti, B.K. Dutta, Photocatalytic degradation of model textile dyes in wastewater using ZnO as semiconductor catalyst, J. Hazard. Mater. 112 (2004) 269–278.
[36] V.K. Gupta, R. Jain, S. Agarwal, A. Nayak, M. Shrivastava, Photodegradation of hazardous dye quinoline yellow catalyzed by TiO_2, J. Colloid Interface Sci. 366 (2012) 135–140.
[37] M.A. Rauf, S.S. Ashraf, Fundamental principles and application of heterogeneous photocatalytic degradation of dyes in solution, Chem. Eng. J. 151 (2009) 10–18.
[38] M. Khatamian, Z. Alaji, Efficient adsorption-photodegradation of 4-nitrophenol in aqueous solution by using ZnO/HZSM-5 nanocomposites, Desalination 286 (2012) 248–253.
[39] L.C. Macedo, D.A.M. Zaia, G.J. Moore, H. de Santana, Degradation of leather dye on TiO_2: A study of applied experimental parameters on photoelectrocatalysis, J. Photochem. Photobiol., A 185 (2007) 86–93.
[40] M. Zarei, A.R. Khataee, R. Ordikhani-Seyedlar, M. Fathinia, Photoelectro-Fenton combined with photocatalytic process for degradation of an azo dye using supported TiO_2 nanoparticles and carbon nanotube cathode: Neural network modeling, Electrochim, Acta 55 (2010) 7259–7265.
[41] J.M. Herrmann, Photocatalysis fundamentals revisited to avoid several misconceptions, Appl. Catal., B 99 (2010) 461–468.
[42] B. Neppolian, H.C. Choi, S. Sakthivel, B. Arabindoo, V. Murugesan, Solar/UV-induced photocatalytic degradation of three commercial textile dyes, J. Hazard. Mater. 89 (2002) 303–317.
[43] M.A. Behnajady, H. Eskandarloo, Preparation of TiO_2 nanoparticles by the sol–gel method under different pH conditions and modeling of photocatalytic activity by artificial neural network, Res. Chem. Intermed., doi: 10.1007/s11164–013–1327–5.
[44] V. Petrovič, V. Ducman, S.D. Škapin, Determination of the photocatalytic efficiency of TiO_2 coatings on ceramic tiles by monitoring the photodegradation of organic dyes, Ceram. Int. 38 (2012) 1611–1616.

[45] M.A. Rauf, M.A. Meetani, S. Hisaindee, An overview on the photocatalytic degradation of azo dyes in the presence of TiO_2 doped with selective transition metals, Desalination 276 (2011) 13–27.
[46] A.P. Toor, A. Verma, C.K. Jotshi, P.K. Bajpai, V. Singh, Photocatalytic degradation of Direct Yellow 12 dye using UV/TiO_2 in a shallow pond slurry reactor, Dyes Pigm. 68 (2006) 53–60.
[47] M.A. Behnajady, S.G. Moghaddam, N. Modirshahla, M. Shokri, Investigation of the effect of heat attachment method parameters at photocatalytic activity of immobilized ZnO nanoparticles on glass plate, Desalination 249 (2009) 1371–1376.
[48] N. Daneshvar, M.H. Rasoulifard, A.R. Khataee, F. Hosseinzadeh, Removal of C.I. Acid Orange 7 from aqueous solution by UV irradiation in the presence of ZnO nanopowder, J. Hazard. Mater. 143 (2007) 95–101.
[49] B. Esen, T. Yumak, A. Sınağ, T. Yıldız, Investigation of photocatalytic effect of SnO_2 nanoparticles synthesized by hydrothermal method on the decolorization of two organic dyes, Photochem. Photobiol. 87 (2011) 267–274.
[50] A.R. Khataee, H. Aleboyeh, A. Aleboyeh, Crystallite phase-controlled preparation, characterisation and photocatalytic properties of titanium dioxide nanoparticles, J. Exp. Nanosci. 4 (2009) 121–137.